ACS APPLIED MATERIALS & INTERFACES

Research Article

www.acsami.org

Facile Synthesis of Graphene-Wrapped Honeycomb MnO_2 Nanospheres and Their Application in Supercapacitors

Jiayi Zhu[†,‡] and Junhui He*[,†]

[†]Functional Nanomaterials Laboratory and Key Laboratory of Photochemical Conversion and Optoelectronic Materials, Chinese Academy of Sciences, Zhongguancundonglu 29, Haidianqu, Beijing 100190, China

[‡]Graduate University of Chinese Academy of Sciences, Beijing 100049, China

Supporting Information

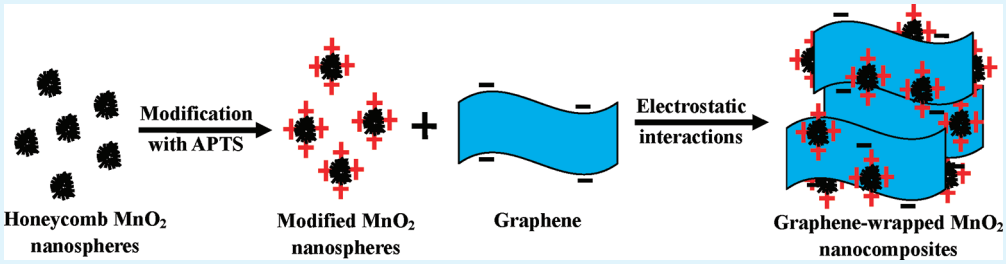

ABSTRACT: Graphene-wrapped MnO_2 nanocomposites were first fabricated by coassembly between honeycomb MnO_2 nanospheres and graphene sheets via electrostatic interaction. The materials were characterized by means of X-ray diffraction, scanning electron microscopy, transmission electron microscopy, atomic force microscopy, and thermogravimetric analysis. The novel MnO_2/graphene hybrid materials were used for investigation of electrochemical capacitive behaviors. The hybrid materials displayed enhanced capacitive performance (210 F/g at 0.5 A/g). Additionally, over 82.4% of the initial capacitance was retained after repeating the cyclic voltammetry test for 1000 cycles. The improved electrochemical performance might be attributed to the combination of the pesudocapacitance of MnO_2 nanospheres with the honeycomb-like "opened" structure and good electrical conductivity of graphene sheets.

KEYWORDS: *monodisperse MnO_2 nanospheres, graphene sheets, nanocomposites, electrostatic interaction, honeycomb-like "opened" structure, supercapacitors*

1. INTRODUCTION

Supercapacitors are charge-storage devices that have been attracting tremendous attention due to their high power density, excellent reversibility and long cycle life.[1] Most research has focused on the development of different electrode materials such as various forms of carbon,[2] conducting polymers,[3] and transition metal oxides.[4]

Among all the materials, manganese dioxide is considered as a good candidate for supercapacitors because of its electrochemical behavior, low cost, and environmental compatibility.[5] Varied methods have been reported to synthesize MnO_2-based materials with different structures and properties, including microemulsion method,[6] hydrothermal reaction,[7] thermal decomposition,[8] electro-deposition,[9] and template method.[10] Although there is yet no standard uniform structure and morphology available for MnO_2 materials in supercapacitors, it is highly desired to develop a rational design to maximize their electrochemically active sites for redox reactions through obtaining "opened" structures to further increase their energy storage density.[11] Recently, we synthesized monodisperse honeycomb MnO_2 nanospheres via microemulsion method,[6] which were used as catalysts for oxidative decomposition of formaldehyde. To the best of our knowledge, however, the monodisperse honeycomb MnO_2 nanospheres synthesized by the microemulsion method have not been used so far as electrode materials for supercapacitors.

Nevertheless, MnO_2 does not usually deliver ideal specific capacitance because of its poor electrical conductivity and electrochemical dissolution during cycling.[12] To circumvent these obstacles, carbonaceous materials with high electrical conductivity and buffer matrix have been widely chosen as matrices for MnO_2-based materials to improve their conductivity and stability.[13−15] Compared to other carbon matrices such as graphite, carbon black, and carbon nanotubes, graphene is emerging as one of the most appealing carbon materials because of its unique properties such as superior electrical conductivity, excellent mechanical flexibility, and high thermal and chemical stability.[16] In the synthesis of hybrid materials for lithium ion batteries, a graphene coating, which is conductive and flexible, was used for preventing inner active materials from electrochemical dissolution as well as improving the electrical conductivity of electrode materials, such as Co_3O_4/graphene,[17] Fe_3O_4/graphene,[18] and Mn_3O_4/graphene.[19]

Received: January 3, 2012
Accepted: February 13, 2012
Published: February 13, 2012

   dx.doi.org/10.1021/am3000165 | ACS Appl. Mater. Interfaces 2012, 4, 1770−1776

Scheme 1. Schematic Illustration for the Synthesis of GW-MnO_2 Nanocomposites

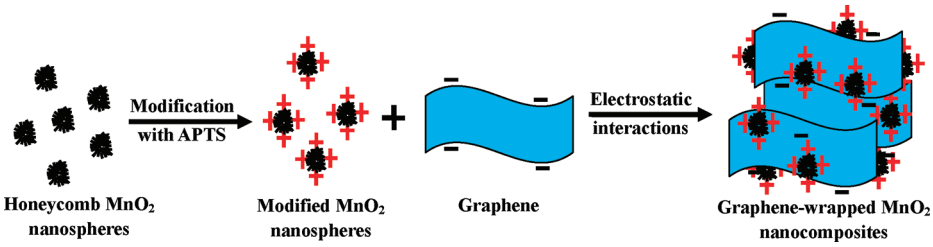

The self-assembly of charged nanomaterials via electrostatic interactions is a controllable route for generating hybrid materials in an aqueous environment.[20,21] It can be considered as a promising candidate for synthesizing electrode materials, in which the electrostatic attractive interactions between oppositely charged nanomaterials are employed to create the robustness of hybrid materials. The layer-by-layer (LbL) electrostatic assembly is one of typical examples, which has been extensively investigated in the past decade.[20] In a very recent study, Zhang and co-workers[22] prepared MnO_2/graphene hybrid materials (FRGO-p-MnO_2) by dispersing negatively charged MnO_2 sheets on functionalized RGO sheets via an electrostatic coprecipitation method.

Herein, we prepared monodisperse MnO_2 nanospheres with a honeycomb-like "opened" structure. The novel graphene-wrapped MnO_2 nanocomposites (GW-MnO_2 nanocomposites) were synthesized by coassembly between positively charged honeycomb MnO_2 nanospheres and negatively charged graphene sheets. The process was driven by electrostatic interactions between the two species. The electrochemical properties of the GW-MnO_2 nanocomposites were investigated in detail, and obtained results revealed that the hybrid materials had a good electrochemical performance as electrode materials for supercapacitors.

2. EXPERIMENTAL SECTION

2.1. Preparation of Honeycomb MnO_2 Nanospheres. In a typical procedure,[6] 1 g of $KMnO_4$ was dissolved in 500 mL of distilled water, and the mixture was stirred for about 0.5 h. A total of 10 mL of oleic acid was added, and a steady emulsion was formed. After the emulsion was maintained at room temperature for 24 h, a brown-black product was collected, and washed several times with distilled water and alcohol to remove any possible residual reactants. Finally, the product was dried in air at 60 °C for 12 h.

2.2. Preparation of Graphene Dispersion. In a typical preparation, graphene oxide (GO) was prepared from natural graphite by using a modified Hummers method.[23] To synthesize graphene dispersion,[24] GO (0.5 mg/mL) was diluted with 80 mL of deionized water under sonication. After 5 min, 40 μL of hydrazine solution (35%) and 280 μL of ammonia solution (25%) was added to the GO dispersion. Subsequently, the mixture was stirred at 90 °C for 1 h. After cooling to room temperature, the black homogeneous dispersion was separated by centrifugation and used for the following fabrication of composites.

2.3. Electrostatic Assembly of Graphene-Wrapped MnO_2 nanocomposites. As illustrated in Scheme 1, honeycomb MnO_2 nanospheres were first reacted with aminopropyltrimethoxysilane (APTS) to modify their surface with NH_2 groups.[17] honeycomb MnO_2 nanospheres (0.25 g), APTS (0.5 mL), and toluene (80 mL) were added successively into a 250 mL round-bottomed flask. The reaction mixture was stirred and refluxed at 120 °C under N_2 for 6 h. The modified MnO_2 nanospheres were then washed with toluene, and dried in air at 60 °C.

The self-assembly of graphene sheets and honeycomb MnO_2 nanospheres was carried out by electrostatic interactions. Briefly, 30 mL of modified honeycomb MnO_2 nanospheres dispersion (3 mg/mL) was added into 30 mL of graphene dispersion (0.3 mg/mL) under mild magnetic stirring. The mixture was stirred at room temperature for 1 h. The GW-MnO_2 nanocomposites were obtained after centrifugation and washing with water. The obtained GW-MnO_2 nanocomposites were finally dried in air at 60 °C. In the synthetic procedure of the hybrid materials, the feeding fractions of MnO_2 and graphene were 90.9% and 9.1%, respectively.

2.4. Characterization. Samples were characterized using powder X-ray diffraction (XRD) on a Philip X'Pert PRO SUPER ç A rotation anode with Ni-filtered Cu KR radiation (λ = 1.5418 Å) at a step size of 0.1°per second. Thermogravimetric analysis (TGA) data were collected on a thermal analysis instrument (NETZSCH STA 449C) with a heating rate of 10 °C/min in an air flow of 50 mL/min. The morphologies of samples were characterized by scanning electron microscopy (SEM) on a Hitachi S-4300 scanning electron microscope operated at 10 kV. Transmission electron microscopy (TEM) images and selected area electron diffraction (SAED) patterns were achieved on a JEOL JEM-2010 transmission electron microscope operated at an acceleration voltage of 150 kV. The surface topology of the graphene sheet was investigated using atomic force microscopy (Nano First SPM, Suzhou Haizisi Nanotechnology Co.) in tapping mode under dry condition. The graphene dispersion was drop-dispensed onto silicon wafer, and dried for AFM observation. The zeta-potential measurements of graphene sheets and honeycomb MnO_2 nanospheres were carried out by means of Malvern Zetasizer 3000HSA equipped with a 633 nm laser. The pH values of the colloidal suspensions were adjusted by using ammonia solution or dilute sulfuric acid. UV−vis absorption spectra were recorded using a TU-1901 spectrophotometer (Beijing Purkinje General Instrument Co.). Fourier transform infrared spectra (FTIR) were recorded on a Varian Excalibur 3100 spectrometer. The electrical conductivity of graphene sheets was measured by using the four-point probe method (Guangzhou Four Probes Tech Co).

2.5. Electrochemical Measurements. All electrochemical experiments were carried out using a three-electrode system at room temperature. For making a working electrode, as-prepared materials (GW-MnO_2 nanocomposites and honeycomb MnO_2 nanospheres), acetylene black and polyvinylidene difluoride (PVDF) with a weight ratio of 7:2:1 were pasted on a platinum substrate to form a very homogeneous film with a surface density of 1 mg/cm^2. Before electrochemical tests, the prepared electrodes were soaked overnight in 1 M Na_2SO_4 aqueous solution. Electrochemical measurements were carried out with 1 M Na_2SO_4 aqueous solution as the electrolyte. A platinum foil and a saturated calomel electrode (SCE) were used as the counter and reference electrodes, respectively. All cyclic voltammetry (CV) and galvanostatic charge/discharge were performed on a CHI 660D workstation.

3. RESULTS AND DISCUSSION

3.1. Structure Characterizations. Figure 1 shows XRD patterns of graphene sheets, honeycomb MnO_2 nanospheres, and GW-MnO_2 nanocomposites. After the chemical reduction of GO, a broad peak around 25° could be seen for graphene (Figure 1a). This peak is due to the deep reduction of GO, indicating that most oxygen functional groups had been removed.[5,22] For honeycomb MnO_2 nanospheres (Figure 1b), significant XRD peaks were recorded at 2θ = 12.3, 24.3, 36.6, and 65.7°, and could be well-assigned to the (001), (002), (100), and (110) planes of birnessite-type MnO_2, respectively.

dx.doi.org/10.1021/am3000165 | ACS Appl. Mater. Interfaces 2012, 4, 1770−1776

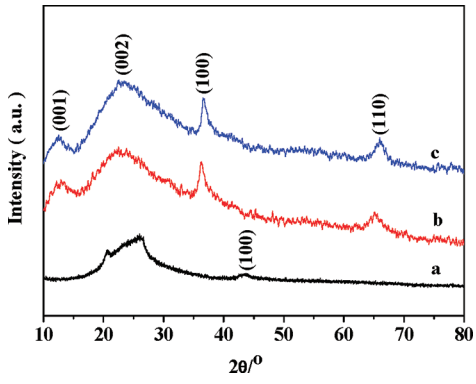

Figure 1. (a) XRD patterns of graphene sheets, (b) honeycomb MnO_2 nanospheres, and (c) the GW-MnO_2 nanocomposites.

From 2θ = 12.3°, the interlayer spacing was estimated to be ca. 0.72 nm, in good agreement with the literature.[6,25,26] The (001) reflection at 2θ = 12.3° was used to estimate the thickness of the MnO_2 nanoplatelet by the Scherrer equation.[6] The obtained results showed that the MnO_2 nanoplatelet had a thickness of ca. 4.3 nm. Thus, the MnO_2 nanoplatelet was supposed to consist of 3–4 MnO_2 monolayers. The GW-MnO_2 nanocomposites show an XRD pattern (Figure 1c) similar to that of honeycomb MnO_2 nanospheres. However, the peak at 2θ of ca. 43° corresponding to the (100) crystal plane of graphene could not be observed clearly,[5] suggesting that the self-assembly process with a low fraction of graphene does not affect the crystal structure of honeycomb MnO_2 nanospheres. Nevertheless, the addition of graphene sheets is believed to enable electrical conductivity of the hybrid materials.

Figure 2 shows FTIR spectra of honeycomb MnO_2 nanospheres. Before amination (Figure 2a), the absorption band at

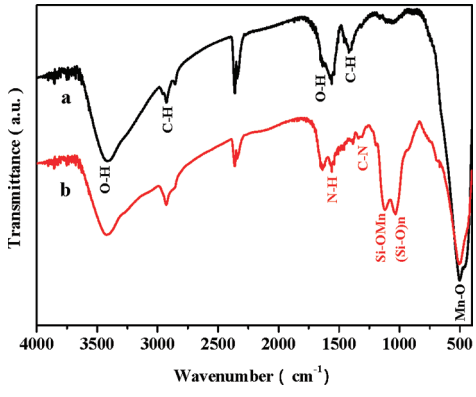

Figure 2. FTIR spectra of (a) as-prepared and (b) APTS modified honeycomb MnO_2 nanospheres.

519 cm^{-1} is assigned to the Mn–O stretching vibration; the band at 3450 cm^{-1} corresponds to the O–H stretching vibration of water molecule and OH^- in the lattice; the band at 1640 cm^{-1} derives from the O–H bending vibration of adsorbed water molecules. The bands at 1421 and 2935 cm^{-1} are assigned to the C–H bending or stretching vibrations of oleic acid, indicating the existence of a little oleic acid in honeycomb MnO_2 nanospheres.[27] After the amination reaction (Figure 2b), compared with the as-prepared honeycomb MnO_2 nanospheres, the bands attributed to the Mn–O stretching vibration at 519 cm^{-1} and C–H bending vibration at 1421 cm^{-1} decrease, and several additional absorption bands at 1040, 1130, 1370, and 1570 cm^{-1} appear, which are assigned to the (Si–O)n, Si-OMn, C–N, and N–H stretching or bending vibrations, respectively.[17] It suggests that APTS moieties had been successfully grafted onto the surface of honeycomb MnO_2 nanospheres during the modification process.

The morphology and structure of honeycomb MnO_2 nanospheres, graphene sheets, and GW-MnO_2 nanocomposites were elucidated by SEM and TEM observations (Figure 3). As

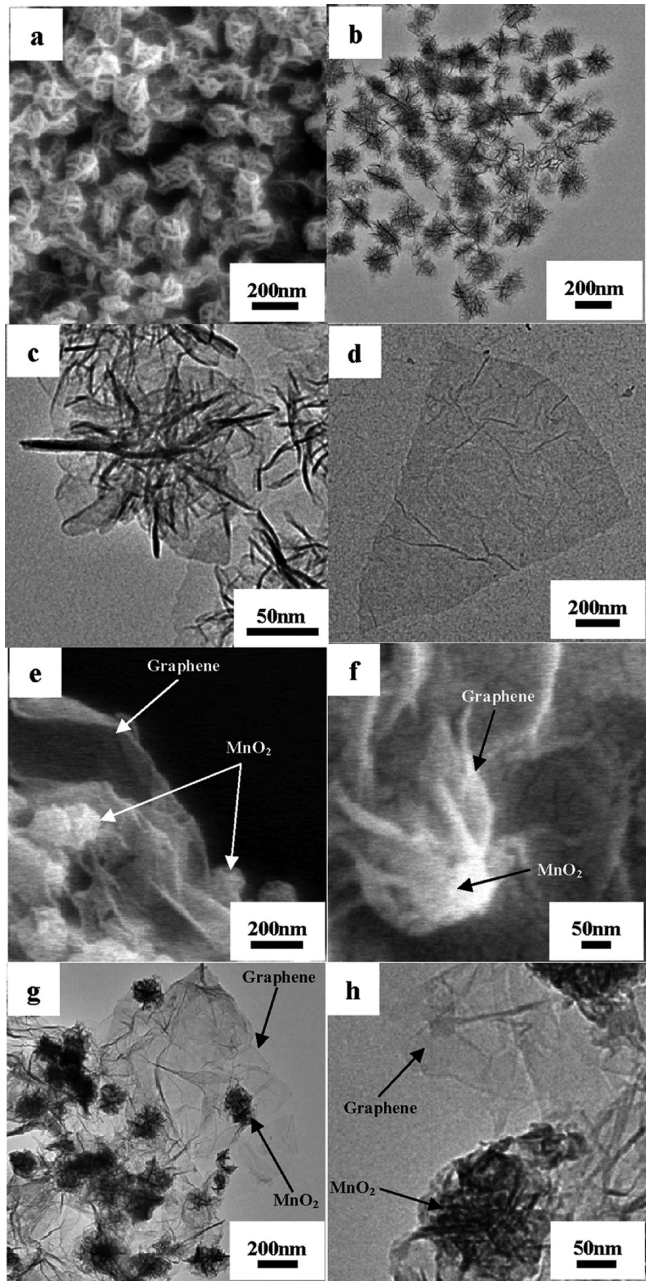

Figure 3. (a–c) SEM and TEM images of honeycomb MnO_2 nanospheres. (d) TEM images of graphene sheets. (e–h) SEM and TEM images of GW-MnO_2 nanocomposites.

seen from images a and b in Figure 3, the MnO_2 nanospheres of ca. 100 nm in diameter have a honeycomb-like structure that was formed by the self-assembly of MnO_2 nanoplatelets.[6] A magnified TEM image (Figure 3c) shows that each nanosphere consists of nanoplatelets that self-align perpendicular to the sphere surface and emanate from the center rather like the

dx.doi.org/10.1021/am3000165 | ACS Appl. Mater. Interfaces 2012, 4, 1770–1776

structure of honeycomb. Figure 3d shows that graphene sheets are transparent as thin layers.[28,29] Many wrinkles and folds reveal that the two-dimensional structure of graphene sheets is flexible. The average thickness of the graphene sheet was also measured from the height profile of AFM image, and was estimated to be ca. 0.86 nm, which indicates the perfect platelet structure of single sheet graphene (see Figure S1 in the Supporting Information). SAED measurements yielded well-defined 6-fold-symmetry diffraction (see Figure S2a in the Supporting Information).[30] UV−visible absorption spectra (Figure S2b, Supporting Information) show that the absorption peak of the GO dispersion at 229 nm red-shifted to 265 nm after the reduction reaction, suggesting that the electronic conjugation within the graphene sheets was restored upon hydrazine reduction. Thus, GO was successfully reduced to flexible and conductive graphene.[31] The GW-MnO_2 nanocomposites show crinkled and rough textures, which is associated with the presence of flexible and ultrathin graphene sheets (Figure 3e). A magnified image (Figure 3f) shows that honeycomb MnO_2 nanospheres are wrapped by flexible and ultrathin graphene sheets, which would help to not only enable electrical conductivity of the nanocomposites but also prevent honeycomb MnO_2 nanospheres from electrochemical dissolution. TEM image (Figure 3g) reveals that these honeycomb MnO_2 nanospheres are firmly attached to graphene sheets even after ultrasonication used to disperse the GW-MnO_2 nanocomposites for TEM characterization, indicating the strong electrostatic interactions between honeycomb MnO_2 nanospheres and graphene sheets. Magnified TEM image (Figure 3h) shows the edges of individual graphene layers and the honeycomb-like "opened" structure of MnO_2 nanospheres.[32]

On the basis of the above analyses, a plausible synthetic procedure was proposed and shown in Scheme 1. Honeycomb MnO_2 nanospheres were first prepared via microemulsion method,[6] and then modified by APTS moieties to render the honeycomb MnO_2 nanospheres surface positively charged.[33] The modified honeycomb MnO_2 nanospheres were then assembled with negatively charged graphene sheets by electrostatic interactions. Notably, to obtain complementarily switched opposing charges of graphene sheets and the modified honeycomb MnO_2 nanospheres for electrostatic assembly,[17,28] the modified honeycomb MnO_2 nanospheres suspension was adjusted to pH 2 for a positive zeta potential of +20.1 mV, which also revealed the successful grafting of APTS moieties onto the surface of honeycomb MnO_2 nanospheres, and the graphene dispersion was adjusted to pH 9 for a negative zeta potential of −30.3 mV, as listed in Table 1. Under the above optimal conditions, almost all the graphene sheets and modified honeycomb MnO_2 nanospheres coassembled to leave a transparent aqueous solution (see Figure S3 in the Supporting Information),[17] resulting in GW-MnO_2 nanocomposites.

Table 1. Average Zeta Potentials of Samples Measured at 25 °C

samples	pH	zeta potential (mV)
graphene	9.0	−30.3
modified MnO_2	2.0	+20.1

TGA analysis (Figure 4) was used to determine the actual fractions of graphene and MnO_2 in GW-MnO_2 nanocomposites. The weight loss of 7.7% below 200 °C is attributed to the removal of surface-adsorbed water, and the weight loss of

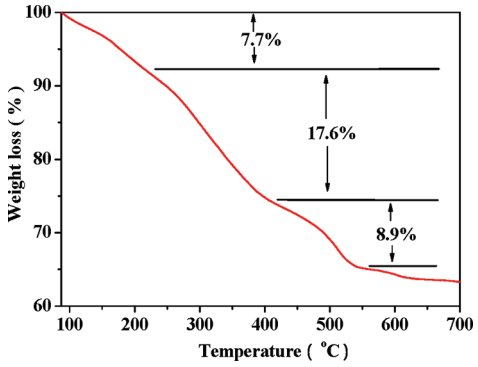

Figure 4. TGA curve of the GW-MnO_2 nanocomposites.

17.6% in the temperature range of 200−410 °C corresponds to the release of adsorbed oleic acid and water in the lattice.[27] As manganese oxide does not have weight loss between 415 and 540 °C,[4,22] the weight loss of 8.9% in the temperature range should be attributed to the removal of carbon sketch by burning of graphene,[34,35] and thus the actual fraction of MnO_2 and graphene in the initial nanocomposites is 91.1% and 8.9%, which are very similar to the feeding fractions of MnO_2 (90.9%) and graphene (9.1%) in the synthetic procedure of the hybrid materials. This similarity suggests that the electrostatic assembly process could easily and accurately control the actual fractions of MnO_2 and graphene in the initial nanocomposites by the feeding fractions of two components, as compared with other redox reactions.[5,18] The small weight loss above 550 °C is attributed to the slight phase transformation of manganese oxide.[22,32] Such a high content of MnO_2 nanospheres with the honeycomb-like "opened" structure in the hybrid materials, in association with flexible, conductive graphene coatings as the conducting pathways and protecting matrix, might result in high capacity and excellent cycling performance when they are applied to supercapacitors.

3.2. Electrochemical Properties. The capacitive performances of materials were evaluated by cyclic voltammetry (CV) and galvanostatic charge/discharge techniques in 1 M Na_2SO_4 aqueous solution.[36]

CV is a suitable tool to characterize the capacitive behavior of electrode materials. As seen from Figure 5a, GW-MnO_2 nanocomposites have a rectangle-shaped and symmetric CV curve at a low scan rate of 10 mV/s, indicating their perfect capacitive behavior.[4,37] The CV current density increases gradually with increase of the scan rate, but the CV curves do not always maintain an rectangular shape, especially at a high scan rate. It can be attributed to the fact that the charging−discharging process of GW-MnO_2 nanocomposites in the Na_2SO_4 aqueous electrolyte is mainly governed by the insertion of Na^+ from the electrolyte into the hybrid material and its release from the nanocomposites to the electrolyte.[4] At a low scan rate of 10 mV/s, the Na^+ ion can easily diffuse into almost all available space of the hybrid material, leading to a sufficient insertion reaction and showing almost perfect capacitive behavior. However, increasing the scan rate has a remarkable impact on the diffusion of Na^+ into the hybrid material. At a high scan rate of 100 mV/s, the Na^+ ion can only approach the outer surface of the hybrid material and the material located in the deep space has little contribution to the electrochemical capacitive behavior, leading to the deviation from the ideal rectangular shape of the CV curve. Average capacitances (C_a) were calculated according to $C_a = (\int IdV)/(mVv)$, where I is

dx.doi.org/10.1021/am3000165 | ACS Appl. Mater. Interfaces 2012, 4, 1770−1776

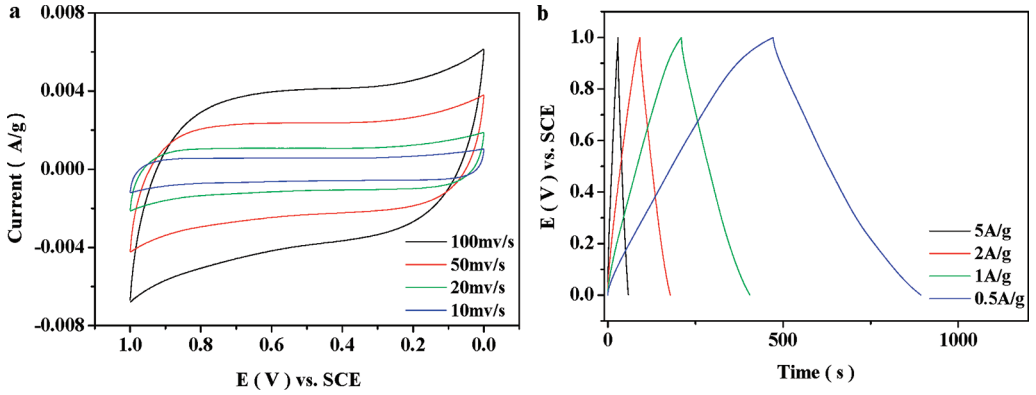

Figure 5. (a) CV curves of GW-MnO_2 nanocomposites at different scan rates of 10, 20, 50, and 100 mV/s. (b) Galvanostatic charge/discharge curves of GW-MnO_2 nanocomposites at different current densities of 0.5, 1, 2, and 5 A/g.

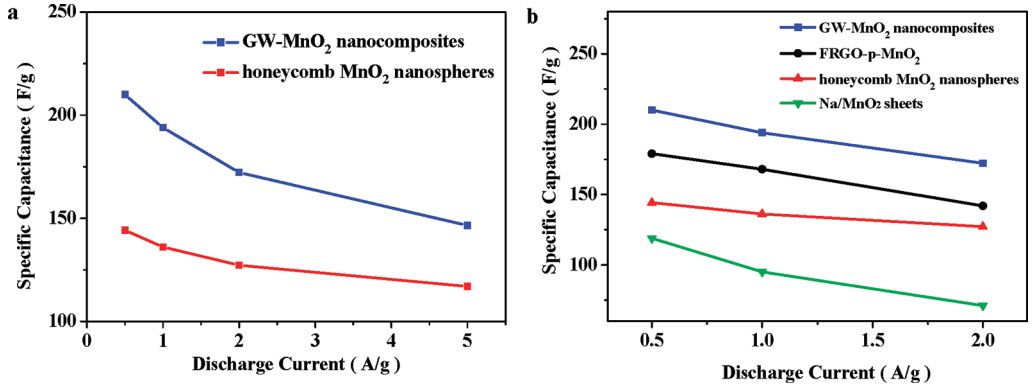

Figure 6. (a) Specific capacitances of GW-MnO_2 nanocomposites and honeycomb MnO_2 nanospheres at different discharge currents (0.5−5A/g) in 1 M Na_2SO_4 solution. (b) Specific capacitances of GW-MnO_2 nanocomposites, FRGO-p-MnO_2, honeycomb MnO_2 nanospheres and Na/MnO_2 sheets at different current densities (0.5−2A/g).

the response current density, V is the potential window, υ is the potential scan rate, and m is the mass of the active material in the electrode.[5] They are 170, 154, 125, and 100 F/g at the scan rates of 10, 20, 50, and 100 mV/s, respectively.

To assess the potential of GW-MnO_2 nanocomposites as electrode materials for supercapacitors, galvanostatic charge/discharge measurements were also carried out. As illustrated in Figure 5b, during the charging and discharging steps, the charge curve of GW-MnO_2 nanocomposites is almost symmetric to its corresponding discharge counterpart with a slight curvature, pointing to high reversibility of the hybrid materials.[38] The time of the charging−discharging procedure increases gradually with decrease of the current density, which is attributed to the sufficient insertion or release of Na^+ during the charging and discharging steps. The specific capacitances (C_s) were calculated according to $C_s = (It)/(mV)$, where I is the constant discharge current, V is the potential window, t is the discharge time, and m is the mass of the active material in the electrode.[39] They are 210, 194, 172, and 147 F/g, respectively, at discharge current densities of 0.5, 1, 2, and 5 A/g, respectively.

The specific capacitances of GW-MnO_2 nanocomposites and honeycomb MnO_2 nanospheres at varied current densities (0.5−5 A/g) in 1 M Na_2SO_4 aqueous solution are shown in Figure 6a. The GW-MnO_2 nanocomposites exhibit higher specific capacitances at identical current densities than those of pure honeycomb MnO_2 nanospheres. For example, the GW-MnO_2 nanocomposites display the maximum specific capacitance of 210 F/g at 0.5 A/g, which is much higher than that of pure honeycomb MnO_2 nanospheres (144 F/g). The enhancement of capacitive performance of GW-MnO_2 nanocomposites can certainly be attributed to good electrical conductivity of graphene sheets, which was measured to be ca. 322 S/m. Graphene acts as an electronic conductive channel in the nanocomposites, and is beneficial to the fast transfer of electrons throughout the whole electrode and eventually to the higher electrochemical performance.[5,17]

The capacitive performances of the as-prepared GW-MnO_2 nanocomposites and honeycomb MnO_2 nanospheres were compared with those of previous reported materials.[22,40−42] Figure 6b shows the specific capacitances of GW-MnO_2 nanocomposites (blue line), FRGO-p-MnO_2 (black line),[22] honeycomb MnO_2 nanospheres (red line), and Na/MnO_2 sheets (green line)[22,40] at varied current densities (0.5−2 A/g). Clearly, the GW-MnO_2 nanocomposites display higher specific capacitances than three others, at identical current densities. As seen from Scheme 2, there might be two reasons for the higher electrochemical performance of GW-MnO_2 nanocomposites. One could be attributed to the MnO_2 nanspheres with the honeycomb-like "opened" structure that was formed by the self-assembly of MnO_2 nanoplatelets.[6] Pseudocapacitive reactions between manganese oxides and Na^+ mainly occurred on the surface and in the bulk of the electrode[5,11]

$$MnO_2 + C^+ + e^- \leftrightarrow MnOOC\ (C^+ = H^+, Na^+) \quad (1)$$

Scheme 2. Schematic Illustration for the Charging–Discharging Procedure of GW-MnO_2 Nanocomposites

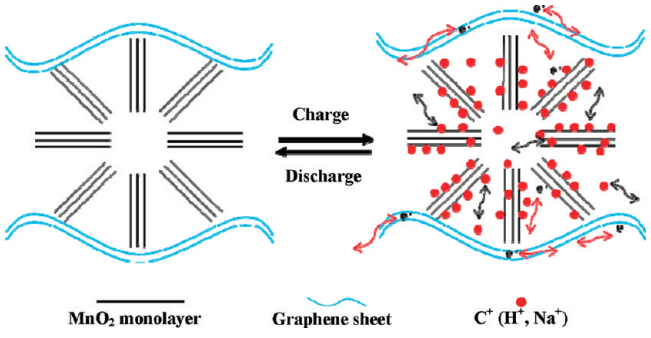

Compared with Na/MnO_2 sheets, the interstitial space between MnO_2 nanoplatelets in the honeycomb-like "opened" structure could not only supply sufficient electrochemically active sites for effective redox reactions on the surface of manganese oxides, but also provide porous channels for the deep intercalation or deintercalation of Na^+ in manganese oxides,[5,11,18] resulting in the higher specific capacitance of honeycomb MnO_2 nanospheres. The other could certainly be attributed to the conductive graphene coatings, which could enhance the specific capacitances of pure MnO_2 materials through improving their electrical conductivity.[41,42] As a result, because of the synergistic effect of the pseudocapacitive MnO_2 nanospheres with the honeycomb-like "opened" structure and conductive, flexible graphene sheets, the GW-MnO_2 nanocomposites exhibited the highest specific capacitance.

Additionally, it is noted that the specific capacitance of honeycomb MnO_2 nanospheres levels off with increase of the current density but that of Na/MnO_2 sheets decreases quickly. This might be because that the honeycomb-like "opened" structure of MnO_2 nanospheres could be beneficial to the fast adsorption of Na^+ on the surface of manganese oxides through the interstitial space, and thus maintain the sufficient electrochemical reactions between MnO_2 and electrolyte cations even at the higher current density within short time. Thus, it could reduce the loss of specific capacitance with increase of the current density as compared with Na/MnO_2 sheets.[22,40]

The electrochemical stability of GW-MnO_2 nanocomposites was further investigated in the range of 0–1 V at 10 mV/s in 1 M Na_2SO_4 aqueous solution. As shown in Figure 7 (black arrow),

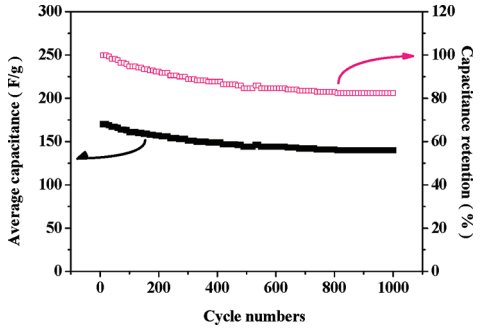

Figure 7. Capacitance retention of GW-MnO_2 nanocomposites in the range of 0–1 V at 10 mV/s in 1 M Na_2SO_4 aqueous solution.

the initial average capacitance (first cycle) of GW-MnO_2 nanocomposites was 170 F/g, and it decreased to 140 F/g after 1000 cycles. Compared to the first cycle, the capacitance retained about 82.4% of the initial capacitance after 1000 charge-dischange cycles, indicating a good cycling stability of the hybrid material (pink arrow). Herein, graphene might play a "flexible confinement" role to enwrap honeycomb MnO_2 nanospheres,[43] and prevent honeycomb MnO_2 nanospheres from electrochemical dissolution,[44,45] which would contribute to the better cycling stability of GW-MnO_2 nanocomposites than bare MnO_2 electrodes[46] and other graphene/MnO_2 composites.[47]

4. CONCLUSIONS

In summary, we have first synthesized the novel GW-MnO_2 nanocomposites by self-assembly of honeycomb MnO_2 nanospheres and graphene sheets via an electrostatic coprecipitation method. It shows that the electrostatic coprecipitation method is a simple and controllable method to synthesize hybrid materials for supercapacitors. Moreover, the GW-MnO_2 nanocomposites exhibited enhanced capacitive performance as high as 210 F/g at 0.5 A/g, which is attributed to the synergistic effect between the pesudocapacitance of honeycomb MnO_2 nanospheres and good electrical conductivity of graphene sheets. The GW-MnO_2 nanocomposites retained about 82.4% of the original capacitance after 1000 cycles of charge–discharge. These results demonstrate exciting potentials of the GW-MnO_2 nanocomposites for high-performance supercapacitors.

■ ASSOCIATED CONTENT

Ⓢ Supporting Information

The method of preparation of graphene oxide; AFM image of a graphene sheet; selected area electron diffraction pattern of graphene and UV–visble absorption spectra of graphene and GO; digital photographs of honeycomb MnO_2 nanospheres suspension, graphene dispersion, and GW-MnO_2 nanocomposites. This material is available free of charge via the Internet at http://pubs.acs.org.

■ AUTHOR INFORMATION

Corresponding Author

*Tel/Fax: +86 10 82543535. E-mail: jhhe@mail.ipc.ac.cn.

Notes

The authors declare no competing financial interest.

■ ACKNOWLEDGMENTS

We thank Dr. X. Zhang and Prof. Y. W. Ma (Institute of Electrical Engineering, Chinese Academy of Sciences, Beijing, P. R. China) for helpful discussions. This work was supported by the National Natural Science Foundation of China (Grant 20871118) and the Knowledge Innovation Program of Chinese Academy of Sciences (CAS) (Grant timetinKGCX2-YW-370, KGCX2-EW-304-2). It was also partially supported by Key Laboratory of Photochemical Conversion and Optoelectronic Materials, Technical Institute of Physics and Chemistry (TIPC), CAS.

■ REFERENCES

(1) Simon, P.; Gogotsi, Y. *Nat. Mater.* **2008**, *7*, 845–854.
(2) Chen, Y.; Zhang, X.; Zhang, D.; Yu, P.; Ma, Y. *Carbon* **2011**, *49*, 573–580.
(3) Zhang, D.; Zhang, X.; Chen, Y.; Yu, P.; Wang, C.; Ma, Y. *J. Power Sources* **2011**, *196*, 5990–5996.
(4) Chen, S.; Zhu, J.; Wu, X.; Han, Q. *ACS Nano* **2010**, *4*, 2822–2830.
(5) Yan, J.; Fan, Z.; Wei, T.; Qian, W.; Zhang, M.; Wei, F. *Carbon* **2010**, *48*, 3825–3833.

(6) Chen, H.; He, J.; Zhang, C.; He, H. *J. Phys. Chem. C* **2007**, *111*, 18033−18038.
(7) Xu, M.; Kong, L.; Zhou, W.; Li, H. *J. Phys. Chem. C* **2007**, *111*, 19141−19147.
(8) Yu, C.; Zhang, L.; Shi, J.; Zhao, J.; Gao, J.; Yan, D. *Adv. Funct. Mater.* **2008**, *18*, 1544−1554.
(9) Liu, R.; Lee, S. B. *J. Am. Chem. Soc.* **2008**, *130*, 2942−2943.
(10) Fei, J. B.; Cui, Y.; Yan, X. H.; Qi, W.; Yang, Y.; Wang, K. W.; He, Q.; Li, J. B. *Adv. Mater.* **2008**, *20*, 452−456.
(11) Wei, W.; Cui, X.; Chen, W.; Ivey, D. G. *Chem. Soc. Rev.* **2011**, *40*, 1697−1721.
(12) Fischer, A. E.; Pettigrew, K. A.; Rolison, D. R.; Stroud, R. M.; Long, J. W. *Nano Lett.* **2007**, *7*, 281−286.
(13) Prasad, K. R.; Miura, N. *J. Power Sources* **2004**, *135*, 354−360.
(14) Kim, J.-H.; Lee, K. H.; Overzet, L. J.; Lee, G. S. *Nano Lett.* **2011**, *11*, 2611−2617.
(15) Jin, X.; Zhou, W.; Zhang, S.; Chen, G. Z. *Small* **2007**, *3*, 1513−1517.
(16) Novoselov, K. S.; Geim, A. K.; Morozov, S. V.; Jiang, D.; Zhang, Y.; Dubonos, S. V.; Grigorieva, I. V.; Firsov, A. A. *Science* **2004**, *306*, 666−669.
(17) Yang, S.; Feng, X.; Ivanovici, S.; Müllen, K. *Angew. Chem., Int. Ed.* **2010**, *49*, 8408−8411.
(18) Zhou, G.; Wang, D.-W.; Li, F.; Zhang, L.; Li, N.; Wu, Z.-S.; Wen, L.; Lu, G. Q.; Cheng, H.-M. *Chem. Mater.* **2010**, *22*, 5306−5313.
(19) Wang, H.; Cui, L.-F.; Yang, Y.; Sanchez Casalongue, H.; Robinson, J. T.; Liang, Y.; Cui, Y.; Dai, H. *J. Am. Chem. Soc.* **2010**, *132*, 13978−13980.
(20) Li, Z.; Wang, J.; Liu, X.; Liu, S.; Ou, J.; Yang, S. *J. Mater. Chem.* **2011**, *21*, 3397−3403.
(21) Wang, L.; Wang, D.; Dong, X. Y.; Zhang, Z. J.; Pei, X. F.; Chen, X. J.; Chen, B.; Jin, J. *Chem. Commun.* **2011**, *47*, 3556−3558.
(22) Zhang, J.; Jiang, J.; Zhao, X. S. *J. Phys. Chem. C* **2011**, *115*, 6448−6454.
(23) Hummers, W. S.; Offeman, R. E. *J. Am. Chem. Soc.* **1958**, *80*, 1339−1339.
(24) Li, D.; Muller, M. B.; Gilje, S.; Kaner, R. B.; Wallace, G. G. *Nat. Nanotechnol* **2008**, *3*, 101−105.
(25) Ma, Y.; Luo, J.; Suib, S. L. *Chem. Mater.* **1999**, *11*, 1972−1979.
(26) Feng, Q.; Kanoh, H.; Ooi, K. *J. Mater. Chem.* **1999**, *9*, 319−333.
(27) Chen, H.; He, J. *J. Phys. Chem. C* **2008**, *112*, 17540−17545.
(28) Park, J. S.; Cho, S. M.; Kim, W.-J.; Park, J.; Yoo, P. J. *ACS Appl. Mater. Interfaces* **2011**, *3*, 360−368.
(29) Zhang, S.; Shao, Y.; Liao, H.; Engelhard, M. H.; Yin, G.; Lin, Y. *ACS Nano* **2011**, *5*, 1785−1791.
(30) Zhang, J.; Yang, H.; Shen, G.; Cheng, P.; Zhang, J.; Guo, S. *Chem. Commun.* **2010**, *46*, 1112−1114.
(31) Fan, Z.-J.; Kai, W.; Yan, J.; Wei, T.; Zhi, L.-J.; Feng, J.; Ren, Y.-m.; Song, L.-P.; Wei, F. *ACS Nano* **2010**, *5*, 191−198.
(32) Oh, J.; Lee, J.-H.; Koo, J. C.; Choi, H. R.; Lee, Y.; Kim, T.; Luong, N. D.; Nam, J.-D. *J. Mater. Chem.* **2010**, *20*, 9200−9204.
(33) Liu, J.-W.; Zhang, Q.; Chen, X.-W.; Wang, J.-H. *Chem.—Eur. J.* **2011**, *17*, 4864−4870.
(34) Bao, Q.; Zhang, H.; Yang, J.-x.; Wang, S.; Tang, D. Y.; Jose, R.; Ramakrishna, S.; Lim, C. T.; Loh, K. P. *Adv. Funct. Mater.* **2010**, *20*, 782−791.
(35) Qian, Y.; Lu, S.; Gao, F. *J. Mater. Sci.* **2011**, *46*, 3517−3522.
(36) Wu, Z.-S.; Ren, W.; Wang, D.-W.; Li, F.; Liu, B.; Cheng, H.-M. *ACS Nano* **2010**, *4*, 5835−5842.
(37) Yu, P.; Zhang, X.; Chen, Y.; Ma, Y.; Qi, Z. *Mater. Chem. Phys.* **2009**, *118*, 303−307.
(38) Chen, S.; Zhu, J.; Wang, X. *ACS Nano* **2010**, *4*, 6212−6218.
(39) Wang, Y.-T.; Lu, A.-H.; Zhang, H.-L.; Li, W.-C. *J. Phys. Chem. C* **2011**, *115*, 5413−5421.
(40) Kai, K.; Yoshida, Y.; Kageyama, H.; Saito, G.; Ishigaki, T.; Furukawa, Y.; Kawamata, J. *J. Am. Chem. Soc.* **2008**, *130*, 15938−15943.
(41) Tang, N.; Tian, X.; Yang, C.; Pi, Z. *Mater. Res. Bull.* **2009**, *44*, 2062−2067.
(42) Brousse, T.; Toupin, M.; Dugas, R.; Athouel, L.; Crosnier, O.; Belanger, D. *J. Electrochem. Soc.* **2006**, *153*, A2171−A2180.
(43) Lin, Z.; Liu, Y.; Yao, Y.; Hildreth, O. J.; Li, Z.; Moon, K.; Wong, C.-p. *J. Phys. Chem. C* **2011**, *115*, 7120−7125.
(44) Long, J. W.; Rhodes, C. P.; Young, A. L.; Rolison, D. R. *Nano Lett.* **2003**, *3*, 1155−1161.
(45) McEvoy, T. M.; Long, J. W.; Smith, T. J.; Stevenson, K. J. *Langmuir* **2006**, *22*, 4462−4466.
(46) Ni, J.; Lu, W.; Zhang, L.; Yue, B.; Shang, X.; Lv, Y. *J. Phys. Chem. C* **2008**, *113*, 54−60.
(47) Li, Z.; Mi, Y.; Liu, X.; Liu, S.; Yang, S.; Wang, J. *J. Mater. Chem.* **2011**, *21*, 14706−14711.